

CrossMark
click for updates

Cite this: DOI: 10.1039/c5tc00845j

Multi-modal sensing in spin crossover compounds†

Denis Gentili,^{‡a} Nicola Demitri,^{‡b} Bernhard Schäfer,^c Fabiola Liscio,^d Ilaria Bergenti,^a Giampiero Ruani,^a Mario Ruben^{ce} and Massimiliano Cavallini^{*af}

We exploited the solvatochromic spin-state switching in a spin crossover (SCO) compound based on the Fe^{II} complex and the simultaneous change of spectroscopic properties for selective multimodal sensing of methanol and ethanol. We demonstrate that sensing capabilities are due to the inclusion of methanol or ethanol molecules into the crystalline structure, which tailors simultaneously the transition temperature, colour, birefringence and vibrational modes. We exploited this capability by integrating a neutral compound, switchable at room temperature, into a micrometric TAG sensitive to the colour and birefringence. The system was characterised by optical microscopy, magnetic susceptibility, Raman spectroscopy and X-ray diffraction.

Received 26th March 2015,
Accepted 22nd April 2015

DOI: 10.1039/c5tc00845j

www.rsc.org/MaterialsC

1. Introduction

Spin crossover (SCO) compounds are transition metal complexes capable of switching their spin states upon external stimuli such as temperature, pressure, magnetic field and light.¹ Typically they are formed by a transition metal with 3d⁴–3d⁷ configurations, in which the “d electrons” can be distributed, paired or unpaired, depending on the difference in energy between t_{2g} and e_g* d-orbitals. The switching involves a structural transition that induces a change in d-orbital splitting and consequently the electron redistribution (*viz.* the spin transition), as well as the change of many physical properties such as: colour, magnetic susceptibility, thermal/electric conductivity, dielectric constant, diffraction and mechanical properties.^{2–7} Key parameters for the use of SCO compounds are the transition temperature and the processability, in this respect compounds with transition

temperature close to room temperature and suitable for surface deposition are highly desirable.^{8–10} The SCO phenomenon depends on the molecular packing, crystallinity, anions and eventually on solvent molecules that are often included in the crystal structure.¹¹ The strong influence of these parameters on SCO properties has been largely investigated and summarised in exhaustive reviews.^{3,12–16} SCO properties can be tailored acting on the chemical design of ligands, on the nature and size of counter ions and on the solvent nature;^{13,17,18} a small change in one of these parameters can produce a dramatic change in the transition temperature and associated properties.¹⁹

Thanks to their versatility and multifunctional properties, SCO compounds were proposed for many technological applications, such as molecular memories,^{1,20–22} chemical^{16,23}/pressure²⁴ sensors, and organic electronics,²⁵ among them their use as gas/solvent sensors is probably the most advanced application as recently proposed by Bousseksou's group in a sensor device based on micro-patterned gratings of a SCO molecular organic frameworks.²⁶

Thanks to the variety of properties associated with spin transition and their different responses to external stimuli, SCO compounds offer a unique opportunity for multi-modal sensing (*i.e.* the sensing capability obtained by more than one measurable physical parameter). Here we report on a study of multi-modal sensing capability of a neutral SCO compound used as a selective sensor for methanol and ethanol. We demonstrate that sensing capabilities of a SCO compound are due to the inclusion of alcohol molecules into the crystalline structure of the compound, which tailors the transition temperature and all the associated physical properties. We exploited this capability by integrating a SCO compound into a micrometric TAG sensitive to the change of colour, birefringence and Raman properties.

^a Istituto per lo Studio dei Materiali Nanostrutturati-Consiglio Nazionale delle Ricerche, Via P. Gobetti 101, 40129 Bologna, Italy.
E-mail: massimiliano.cavallini@cnr.it

^b Elettra-Sincrotrone Trieste, S.S. 14 Km 163.5 in Area Science Park, 34149 Basovizza-Trieste, Italy

^c Institute of Nanotechnology, Karlsruhe Institute of Technology, D-76344 Eggenstein-Leopoldshafen, Germany

^d Istituto per la Microelettronica e i Microsistemi-Consiglio Nazionale delle Ricerche, Via P. Gobetti 101, 40129 Bologna, Italy

^e Institut de Physique et Chimie des Matériaux de Strasbourg (IPCMS), CNRS-Université de Strasbourg, 23, rue du Loess, BP 43, 67034, Strasbourg Cedex 2, France

^f Scriba Nanotechnologie S.r.l., Via di Corticella, 183/8 40128 Bologna, Italy

† Electronic supplementary information (ESI) available. CCDC 1055429–1055434.

For ESI and crystallographic data in CIF or other electronic format see DOI: 10.1039/c5tc00845j

‡ DG and ND contributed equally to this manuscript.

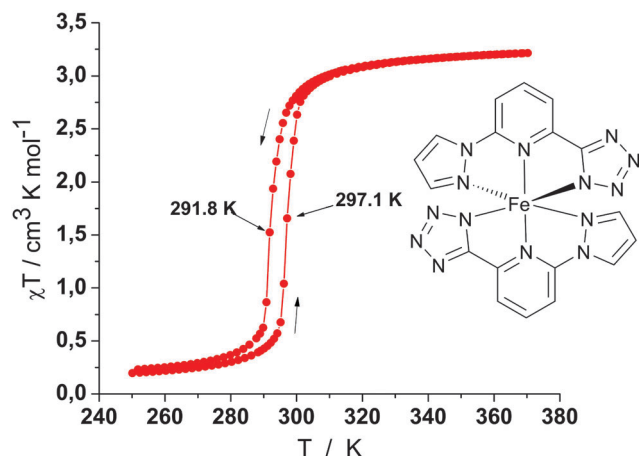


Fig. 1 Magnetic characterization and the structural formula of compound 1.

For our purposes we used SCO complex **1**, with molecular formula $[\text{Fe}(\text{L})_2]$ (LH: (2-(pyrazol-1-yl)-6-(1H-tetrazol-5-yl)pyridine)) (see the chemical structure in the inset of Fig. 1), which is a neutral compound switchable around room temperature whose synthesis and characterization are reported elsewhere.²⁷ As SCO complexes contain Fe^{II} as metal ions, **1** is particularly interesting since it can exist in the diamagnetic state with all electrons paired in t_{2g} orbitals (low spin state, LS) as well as in the paramagnetic state, with four electrons unpaired and distributed between t_{2g} and e_g^* orbitals (high spin state, HS).

2. Results and discussion

2.1 Compound characterization

Complex **1** is a neutral material that crystallizes forming block shaped crystals whose unit cell contains eight complex units $[\text{Fe}(\text{L})_2]$ and ten molecules of methanol.²⁷ Crystals grown from CH_2Cl_2 - CH_3OH solution are yellow in the mother liquor and turn red after the evaporation of the surrounding solvents. Fig. 1 shows the magnetic characterization of the crystalline powder of **1**, which exhibits a transition temperature centred at 295 K with a hysteresis of ~ 5 K that appears after the first thermal cycle.

The spin transition can be followed by polarised optical microscopy (OM) and by Raman spectroscopy. Below the transition temperature the powder of **1** is formed by red crystals of sizes ranging from a few up to 100 μm . Upon heating up to 300 K, the spin state of the powder crosses over from LS to HS accompanied by a colour change from red to yellow/orange.²⁸ The transition is associated with a fragmentation of the crystals, probably due to differences in the crystal structures of low and high spin states. Fig. 2 shows the colour and birefringence evolution of the SCO crystallites upon thermal cycling. Noticeably, when observed by OM with crossed polars, crystallites in the LS state appear to be almost dark (*i.e.* do not show birefringence) while crystallites in the HS state appear to be strongly coloured (*i.e.* show birefringence). Cooling down the sample below the transition temperature the (fragmented) crystals return to red colour and lose the birefringence.

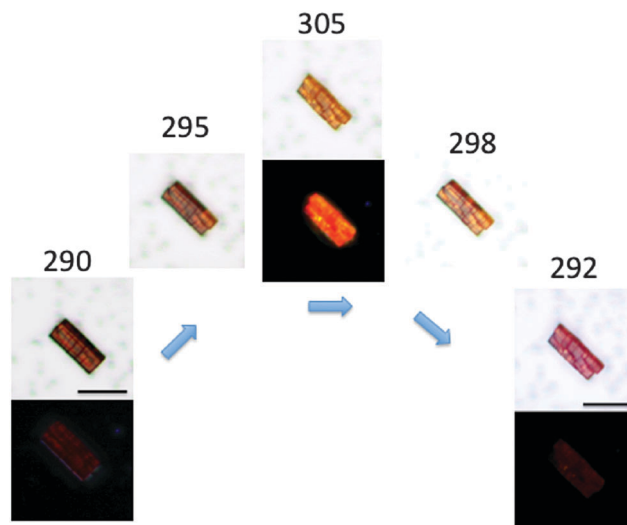


Fig. 2 Real time optical and cross-polarised imaging of the SCO crystallites deposited on silicon upon thermal cycling 290 K \rightarrow 305 K \rightarrow 292 K. Bar is 30 μm . In cross-polarised images, polarizers are oriented parallel and perpendicular to the image axis.

The spin transition of **1** was investigated by μ -Raman spectroscopy, which has been recognized to be an efficient technique for detecting the spin state in SCO compounds.²⁹

The use of μ -Raman, with a small laser spot size (< 1.5 μm), allows the detection of spectra with the resolution of a single crystallite.

According to magnetic and OM characterization methods, Raman spectra were collected at different temperatures, *i.e.* at 280 K, corresponding to complete transformation of **1** in the LS state, and at 328 K, corresponding to complete transformation in the HS state (Fig. 1). The experiments were performed on a single crystal, starting from 294 K then, cooling down to 160 K and subsequently heating up at 328 K and finally cooling again to 280 K. Raman spectra are reversible upon thermal cycling.

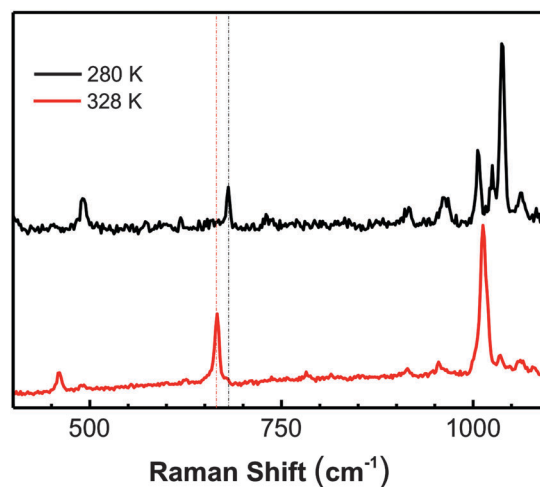


Fig. 3 Raman spectra collected at 328 K and 280 K on a crystallite. The dotted lines indicate the distinctive peak for HS and LS states.

The overall Raman spectrum strongly depends on the molecule spin state showing several distinctive (diagnostic) peaks, mostly concentrated in the range 400–1100 cm^{-1} . Fig. 3 shows the spectra of a specific crystal in the two spin states LS and HS (at 280 K and 328 K, respectively).

Considering the above data, we concluded that the different spin states of **1** can be directly detected by the colour and/or birefringence and/or Raman spectra, in which the red, poor birefringent state corresponds to the LS state and the yellow (orange), highly birefringent state corresponds to the HS state.

2.2 Solvatochromic spin-state-change

Inspired by the fact that the crystals of **1** are in the (yellow) HS state in the mother liquor used for their synthesis and turn to the (red) LS state after the evaporation of the solvents, we exploited the effect of switching on several physical properties for multi-modal sensing of methanol and ethanol.

As **1** is exposed to methanol or ethanol at room temperature the crystals turn from red to yellow as in the thermal spin transition. This effect, named the solvatochromic spin-state change was already observed for several magnetic materials,³⁰ including SCO compounds^{19,31} and is particularly efficient in neutral compounds.²³

The transition occurs both in a vapour atmosphere and in water solution, for a few seconds in the case of methanol and for a few minutes in the case of ethanol. Crystals exposed to methanol switch back to the original red form, in a few seconds, as soon as they are removed from a methanol atmosphere, while crystals exposed to ethanol remain stable in air for a few minutes. No effect was observed by exposing crystallite of **1** to other solvents such as alcohols bigger than ethanol (probably because of the steric hindrance) acetone, dichloromethane, and chloroform for at least 30 minutes.

Fig. 4 shows the behaviour of a crystallite under polarised OM and Raman spectra recorded at room temperature in air, and in a methanol (ethanol) saturated atmosphere. It must be noted that the transition from HS to LS states occurs with a mechanism of nucleation and growth when the crystallites are removed from an alcohol atmosphere. The nucleation preferentially starts at one side of the crystal and propagates to the entire crystal in some ten seconds.

By repeating 10 times the exposure to methanol vapours at room temperature (thus performing the transition from LS to HS states and *vice versa*) no fragmentation was observed. On the other hand, using ethanol, the behaviour of **1**, upon solvent exposure, is more similar to that upon thermal treatment and crystals tend to fragment after a couple of cycles of solvent exposure. As reported below, this fact can be explained by different effects of alcohol on the crystalline structure.

Fig. 5 shows the thermal behaviour of a crystallite at OM in a saturated atmosphere of ethanol. Interestingly, under these conditions a shift of the spin state transition temperature, from 294 K to 248 ± 3 K (272 ± 3 K for methanol) was observed.

The thermal behaviour of crystallites in a methanol-saturated atmosphere was monitored by Raman spectra. Fig. 6 shows the evolution of the diagnostic Raman peaks with the temperature in

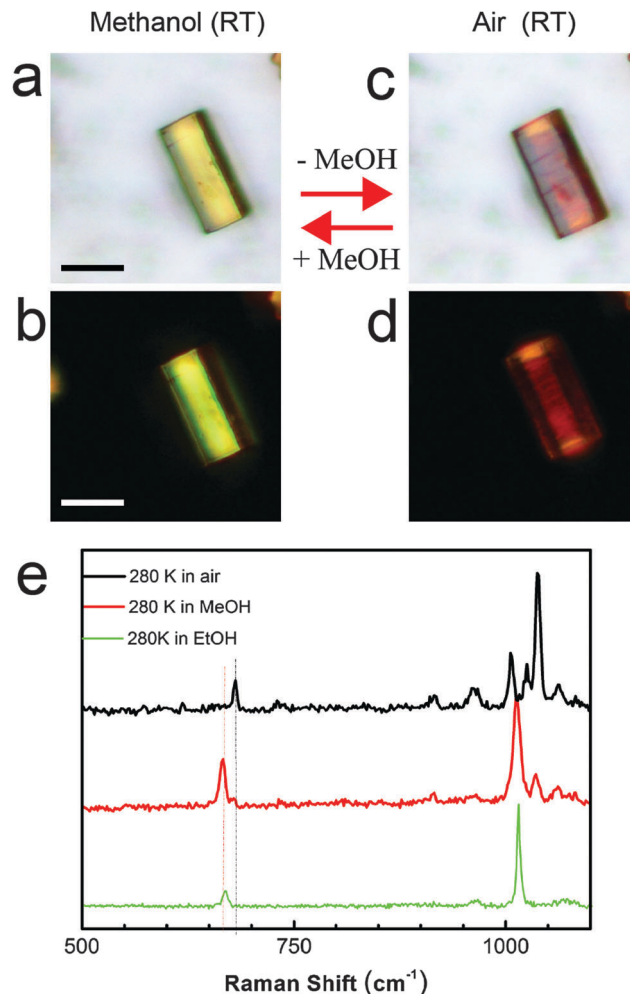


Fig. 4 Bright field and cross-polarized optical images of a crystallite of **1** recorded at room temperature. (a and b) Crystal exposed to the methanol (MeOH) vapours at room temperature; (c and d) the corresponding image of the same crystal in air. (e) Comparison between the Raman spectra in air, in a methanol and an ethanol atmosphere at 280 K.

a methanol-saturated atmosphere that confirms the switching from HS to LS states cooling the sample from room temperature to <255 K. It must be noted that in the case of crystallites exposed to an ethanol atmosphere it was not possible to investigate the thermal behaviour by Raman spectroscopy using our set-up because of ethanol condensation occurring on the sample surface during the cooling process. This condensation led crystallites to fully immerse in ethanol. Under these conditions crystallites do not show thermal transition (we tested starting from 170 K without observing any transition). On the other hand working under OM the measurements are much faster and can be performed limiting the ethanol condensation.

Structural investigation on compound **1** allowed us to obtain atomic level details about alcohol sensing phenomena. X-ray diffraction has been conducted on selected, bigger crystals, which despite the small size were suitable for synchrotron X-ray diffraction analysis.

High quality diffraction data have been acquired for three different cases: dried crystals, crystals exposed to methanol and



Fig. 5 Real time optical imaging of the temperature dependence of the colour of a crystallite of **1** deposited on silicon and recorded in a saturated atmosphere of ethanol. The sample was prepared at room temperature in air then it was exposed to an ethanol-saturated atmosphere, cooled at 233 K and then heated again at room temperature.

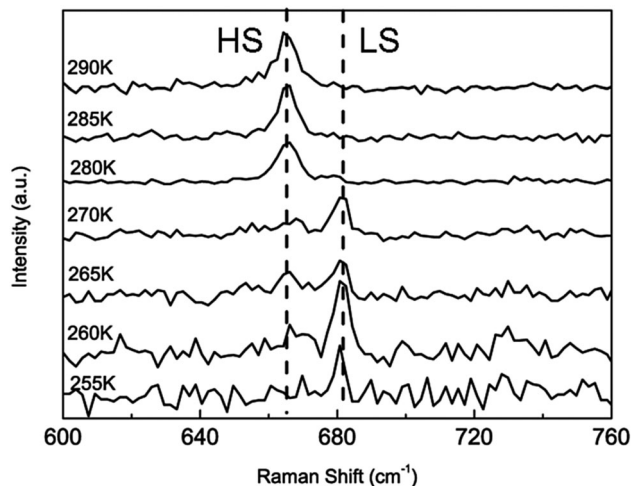


Fig. 6 Temperature evolution of diagnostic Raman peaks of **1** in a saturated atmosphere of methanol vapour.

crystals exposed to ethanol. For each case the temperature has been changed from 300 K down to 100 K using the same crystal (see details of preparation in the Experimental section).

For dried crystals, the structural parameters obtained for the iron complex at both temperatures, are in agreement with data already published for compound **1**.²⁷ A different distribution of disordered solvents in cavities has been found and it has been interpreted with 1.25 water molecules in the asymmetric unit

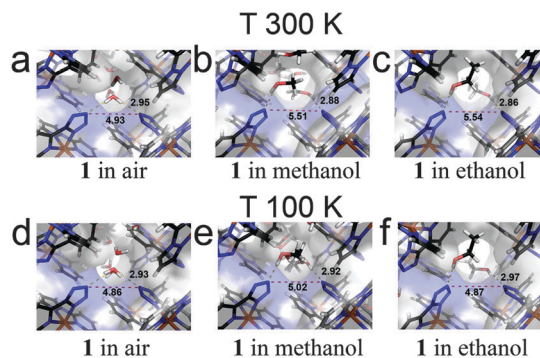


Fig. 7 Partial view of crystal packing showing crystal cavities and solvent molecules in the ASU. Complex **1** molecules are represented with sticks (grey for the ASU molecule and black for symmetry generated ones). (a–c) correspond to structures at 300 K for dried crystals, methanol and ethanol exposed ones. (d–f) correspond to structures at 100 K for dried crystals, methanol and ethanol exposed ones. Hydrogen bonds with tetrazole N10 are shown with yellow dashes, while N10–N10_{sym} distance is represented as red dashes (Å).

(ASU) (Fig. 7a and d). The iron complex show a low spin configuration at both temperatures, as confirmed by the red crystal colour, the iron coordination sphere bond lengths,^{27,32,33} the $N_{\text{pyrazole}}\text{--Fe--}N_{\text{tetrazole}}$ angles close to 160° (ca. 160° for LS and 145° for HS) and the Σ parameter close to 90° (ca. 90° for LS and 160° for HS)^{34,35} (Table 1).

Exposure to methanol converts the red dried crystals to a bright yellow form in a few seconds. The crystals obtained are very prone to switching back to the original red form as soon as the partial pressure of methanol decreases. Crystals exposed to alcohol were quickly dipped in *N*-paratone oil, which limits the methanol loss, and tested by diffraction.

Structural models obtained at 300 K show a significant lengthening of all Fe–N bonds in metal coordination spheres in agreement with an high spin configuration of iron (Table 1 – $N_{\text{pyrazole}}\text{--Fe--}N_{\text{tetrazole}} \cong 160^\circ$ and $\Sigma \cong 160^\circ$).

The superimposition of the models with different iron spin configurations shows significant distortion also in the angle between the L^- ligand molecule planes and the mean iron coordination planes (Fig. 8).

Electron density in the voids shows the presence of methanol molecules; one of them, with full occupancy, is coordinated through a hydrogen bond to N10 nitrogen of the tetrazole ring exposed to crystal cavities (Fig. 7b and e).

The same crystal, cooled to 100 K switches to the red LS state, with a structure equivalent to that of the dried crystal at this temperature.

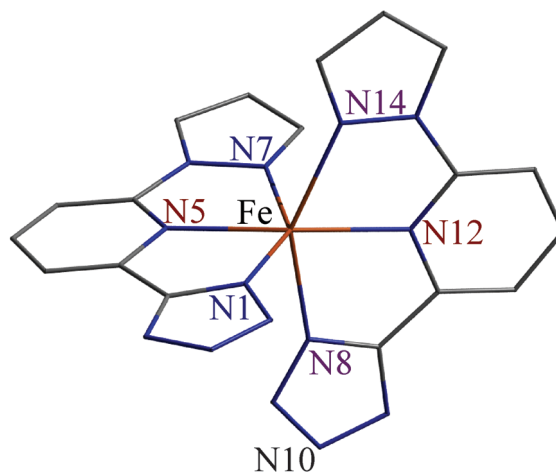
Crystals of **1** exposed to ethanol exhibit a similar transition to those exposed to methanol but with much slower diffusion times and kinetics.

A crystalline model determined at 300 K shows the structural descriptors of a high-spin iron complex with one fully occupied and well-ordered ethanol molecule in the ASU (Fig. 9 and 7c, f).

A LS state is reached upon cooling to 100 K, with a slightly different configuration of the iron coordination sphere compared to the other dataset collected at 100 K. This is probably

Table 1 Bond lengths (Å), significant angles (°) and the naming scheme adopted for iron coordination spheres. The last line reports the distance between tetrazole nitrogen atom N10 of symmetry related molecules; this atom is in close contact with solvent molecules inside crystal cavities

	Dried crystals (published)	Dried crystals	Dried crystals	Crystals with methanol	Crystals with methanol	Crystals with ethanol	Crystals with ethanol
<i>T</i> (K)	180	300	100	300	100	300	100
Fe–N1	1.968(4)	1.978(1)	1.971(5)	2.198(1)	1.970(2)	2.201(2)	1.981(3)
Fe–N7	1.949(4)	1.962(1)	1.968(6)	2.213(1)	1.965(2)	2.210(3)	2.039(3)
Fe–N5	1.916(3)	1.912(1)	1.907(4)	2.144(2)	1.910(2)	2.146(4)	1.929(4)
Fe–N12	1.918(3)	1.912(1)	1.908(4)	2.152(2)	1.912(2)	2.156(5)	1.920(4)
Fe–N8	1.971(4)	1.980(1)	1.975(5)	2.162(1)	1.986(2)	2.159(3)	2.054(3)
Fe–N14	1.959(4)	1.971(1)	1.958(5)	2.204(1)	1.976(2)	2.207(2)	1.991(3)
N1–Fe–N7	160.04(14)	159.75(5)	160.02(19)	147.22(4)	159.91(6)	147.11(10)	159.31(13)
N14–Fe–N8	159.83(14)	159.86(5)	159.92(18)	147.20(5)	159.81(6)	146.77(10)	158.55(12)
Σ^a	87.2	88.6	87.6	148.5	87.5	149.7	105.7
Colour	Red	Red	Red	Yellow	Red	Yellow	Red
Spin states	LS	LS	LS	HS	LS	HS	LS
N10–N10 _{sym}	5.054(5)	4.932(2)	4.864(5)	5.506(5)	5.024(3)	5.540(10)	4.872(7)



$$^a \Sigma = \sum_{i=1}^{12} |\phi_i - 90|, \phi_i \text{ is an N–Fe–N octahedron angle with two N atoms in cis.}$$

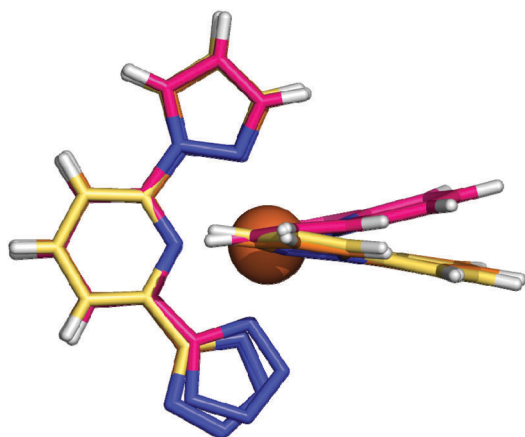


Fig. 8 Superimposition of complex **1** in low spin (dried crystals at 300 K – hot pink sticks) and high spin configurations (methanol exposed crystals at 300 K – orange sticks – and ethanol exposed crystals at the same temperature – yellow sticks).

associated with the increased solvent steric hindrance in the cavities: ethanol-containing voids are higher in this structure compared to methanol and dried ones (Table 2).

The Fe coordination bond lengths found are in agreement with other LS structures of published Fe^{II} complexes bearing nitrogen containing ligands.^{32,33}

After data collection at 100 K all the crystals exposed to alcohol have been heated again up to room temperature recovering the original HS state preserving the methanol/ethanol in the cavities. As expected, the dried crystal remained red going back to 300 K.

As shown in Fig. 7 in all the structures there is a solvent molecule coordinated to a ligand tetrazole ring exposed on the crystal cavity. For dried crystals the N10 coordinated water **1** lies on a twofold axis and is bridging two neighbour complex molecules through hydrogen bonds. In the presence of methanol and ethanol this H-bond crosslink is not possible and this introduces small local changes in the packing. This is in agreement with an ~4% volume increase and ~10% increase between the N10–N10_{sym} distance from low to high spin structures (Table 2).

Assuming that hydrogen bonds between N10 and different alcohols have similar strengths, this packing evidence suggests that the spin crossover phenomena could be mainly lattice driven phenomena. The switching from high spin to low spin states seems to be triggered by bond contractions associated with temperature reduction, while solvent water replacement with

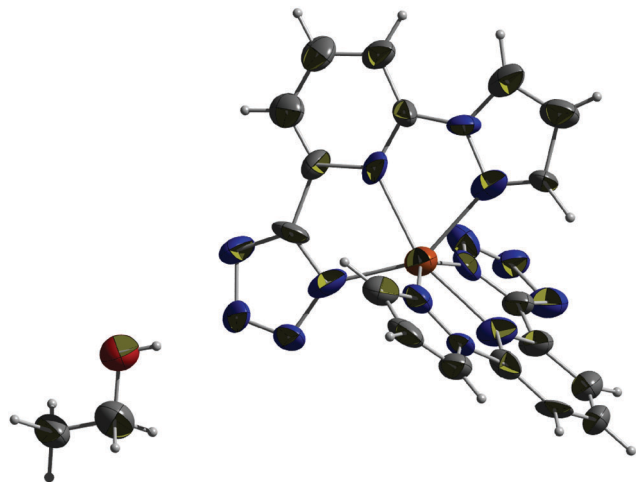


Fig. 9 Asymmetric unit of **1**, crystals exposed to ethanol, obtained by X-ray diffraction at 100 K. Displacement ellipsoids are drawn at 50% probability.

bulkier molecules deforms cavities and increases voids promoting high spin states. Dried crystals' spin state switching to HS at temperature > 300 K is also consistent with this hypothesis assuming that water in channels is removed upon heating.

Complete diffraction data statistics, refinement protocols and further experimental details can be found in the ESI.†

Structural models have been deposited on The Cambridge Crystallographic Data Centre. Access codes are: CCDC 1055429 for molecules **1** in dried crystals (300 K), CCDC 1055430 for dried crystals at 100 K, CCDC 1055431 for crystals exposed to methanol at 300 K, CCDC 1055432 for crystals exposed to methanol at 100 K, CCDC 1055433 for crystals exposed to ethanol at 300 K, CCDC 1055434 for crystals exposed to ethanol at 100 K.

2.3 Multi-modal sensing

This behaviour prompts us to use **1** as a multi-modal sensing material for methanol and ethanol. For this purpose we used the same set-up already used for time temperature integrators TAG, which are devices capable of recording their thermal

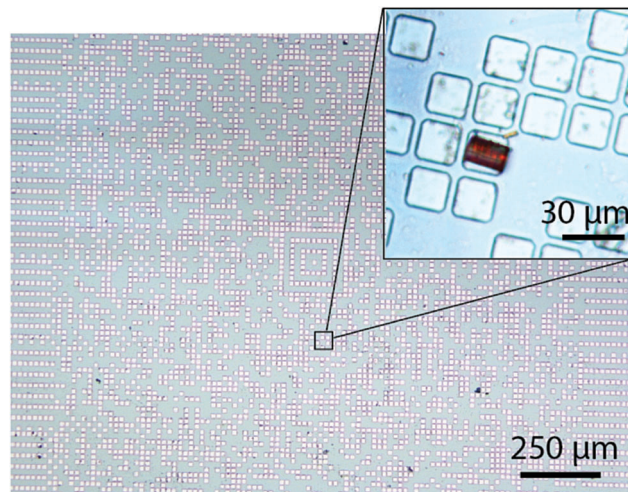


Fig. 10 Optical image of addressable crystallites printed on a micrometric TAG. The position of the crystal is addressable by conventional readers for micro TAGs.

history, by quantitative reading of the colour evolution³⁷ or the birefringence³⁸ directly on micrometric TAGs.³⁹

With this purpose we deposited some crystallites of **1** on a pre-patterned surface. In particular we patterned a TAG containing an Aztec code.³⁷ Patterning of the active material or the pre-fabrication of some markers is necessary in order to make the crystallites addressable, thus readable, using a CCD. Fig. 10 shows an optical image of a crystallite deposited by lithographically controlled wetting^{40,41} into a pre-patterned pixel of a TAG fabricated on the silicon surface.

A commercial CCD is used to record the optical and cross-polarised images of specific crystallites both at room temperature and during the thermal treatment under an alcohol atmosphere.

Fig. 11 shows the number of counts of the red (R), green (G) and blue (B) component recorded using the CCD as a function of the temperature at which the device was exposed for 10 s; each image was recorded fixing the intensity of illumination and the time of acquisition of the CCD (see details in the Method section). The quantitative analysis of the optical images shows that for

Table 2 Unit cell parameters, volumes and basic statistics for different crystals of molecule **1** collected

	Dried crystals (published)	Dried crystals	Dried crystals	Crystals with methanol	Crystals with methanol	Crystals with ethanol	Crystals with ethanol
<i>T</i> (K)	180(2)	300(2)	100(2)	300(2)	100(2)	300(2)	100(2)
<i>a</i> (Å)	23.896(6)	23.784(7)	23.709(1)	24.495(16)	23.843(5)	24.389(49)	23.815(29)
<i>b</i> (Å)	14.9259(19)	14.518(1)	14.472(2)	14.671(3)	14.824(3)	14.586(5)	14.299(5)
<i>c</i> (Å)	15.619(5)	15.534(2)	15.326(49)	16.712(9)	15.571(2)	16.985(21)	17.265(5)
β (°)	129.108(15)	127.854(5)	127.617(14)	131.374(24)	129.178(9)	131.227(38)	131.676(33)
<i>V</i> (Å ³)	4322.5(18)	4235.2(14)	4165(13)	4507(4)	4266.3(13)	4544(11)	4391(6)
Voids <i>V</i> ^a (Å ³)	663.7	562.5	552.3	763.2	638.8	813.0	704.4
Space group	<i>C2/c</i>	<i>C2/c</i>	<i>C2/c</i>	<i>C2/c</i>	<i>C2/c</i>	<i>C2/c</i>	<i>C2/c</i>
<i>R</i> ₁ [<i>I</i> > 2σ(<i>I</i>)]	0.0495	0.0323	0.0756	0.0338	0.0458	0.0514	0.0596
Goof	0.847	1.049	1.110	1.046	1.079	1.030	1.059
Max res. (Å)	0.85	0.72	0.74	0.74	0.72	0.72	0.74
Crystal colour	Red	Red	Red	Yellow	Red	Yellow	Red
Spin states	LS	LS	LS	HS	LS	HS	LS

^a Calculated with a Platon VOID function.³⁶

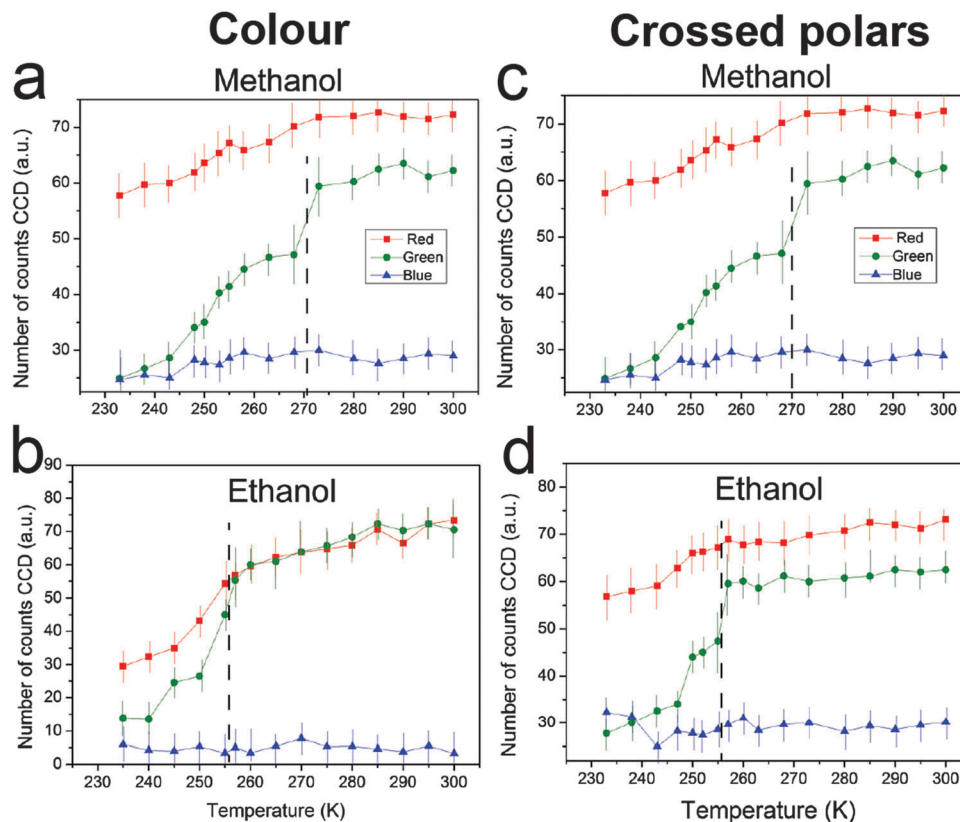


Fig. 11 Quantitative analysis of the optical images. A commercial CCD recorded optical images. The colours of the graphs correspond to the colour components of the CCD (red, blue, green). (a) The number of counts versus temperature obtained for crystals of **1** exposed to a saturated atmosphere of methanol; (b) the number of counts versus temperature obtained for crystals of **1** exposed to a saturated atmosphere of ethanol. Each image was recorded fixing the intensity of illumination and the time of acquisition of the CCD. (c and d) The corresponding number of counts versus temperature obtained in cross-polar images.

each temperature the colour recorded by the CCD is formed by a unique and defined combination of RGB components. The specific colour combination is an interpretation of the CCD, it depends on the particular CCD and illumination and therefore, in order to have a quantitative detection, each CCD must be calibrated. The RGB combination of each colour is itself a way to distinguish whether a crystal is exposed to methanol or ethanol. However a further confirmation was obtained by monitoring the thermal behaviour of crystallites.

In particular we recorded the composition of the colour upon the thermal treatment of **1**.

As shown in Fig. 11, while the red component shows a mean constant decrease upon cooling, the CCD reads the spin transition as a strong change of the green component. The transition is evident from the bright field images and the cross-polar images. It occurs at 270 ± 3 K and at 256 ± 3 K for crystals exposed to methanol and ethanol, respectively. This difference led us to unambiguously discern between methanol and ethanol.

4. Experimental

4.1 Crystallization and alcohol sensing experimental setup

Dried crystals of SCO complex **1**, methanol exposed crystals and ethanol exposed crystals, suitable for diffraction experiments,

have been obtained from a $\text{CH}_3\text{OH}:\text{CH}_2\text{Cl}_2$ 1 : 1 solution by drop casting and slow evaporation (largest size 200 μm), at 4 $^\circ\text{C}$ on Si wafers. Crystals with different habits can be obtained: some have an elongated parallelepiped shape; others appear to have bright red blocks that grow in three dimensions, with more homogeneous lengths. Alcohol interactions have been studied equilibrating the crystals at room temperature (300 K) in Petri dishes. The same results can be detected using vapours or dipping the crystals in liquid alcohol. To limit lattice stress connected to complete solvent removal (crystals dried out) and solvent reintroduction, parts of the crystals have been kept in their mother liquors and transferred to methanol or ethanol, without letting them desolvate.

This approach is useful for methanol but it is not successful for ethanol: electron density maps, which can be obtained using this approach, still show the presence of methanol inside crystal channels (incorporated from the original mother liquors). This result suggested that suitable ethanol sensing experiments had to be done on “activated” fully dried crystals.

Samples deposited on the surface were prepared following the procedures described in ref. 42 and 43.

4.2 Optical microscopy

Optical micrographs were recorded using a Nikon i-80 microscope equipped with epi-illuminator and cross-polars (POM).

The images presented were recorded using objectives: LU Plan ELWD 20×/0.40 and 50×/0.55 objectives. Images were recorded using a commercial CCD (DIGITAL SIGHT DS-2MV).

4.3 Raman spectroscopy

The Nd-YAG excitation wavelength (532 nm) was used to obtain Raman spectra in the 100–2000 cm^{-1} range. Raman scattering measurements were recorded in a backscattering configuration using a long working-distance 50× microscope objective with a laser power lower than 25 μW to avoid photo-thermal effects. The samples were mounted on a Liquid Nitrogen Peltier heating-cooling stage to span the 150–400 K temperature range.

4.4 Thermal treatment and temperature control

The thermal treatments were performed under the optical microscope using a heating stage Linkham TMHS600 connected to a TP94 controller, with a control of 0.1 °C using the setup described in ref. 44.

4.5 X-ray diffraction data collections

Data collections were performed for all these systems at the X-ray diffraction beamline (XRD1) of the Elettra Synchrotron, Trieste (Italy) equipped with a Pilatus 2 M image plate detector. Complete datasets have been collected at a monochromatic wavelength of 0.700 Å through the rotating crystal method. Crystals of **1** and **1** exposed to alcohols were dipped in *N*-paratone, to limit solvent exchange during data acquisition, and mounted on the goniometer head using a nylon loop. The diffraction datasets were collected at controlled temperatures, using a nitrogen stream supplied through an Oxford Cryostream 700: for all the samples, data collected at room temperature and 100 K, from the same crystal are reported in this work. Significant changes have been detected for systems exposed to alcohols as a function of temperature. The diffraction data were indexed, integrated and scaled using XDS.⁴⁵ The structures were solved by direct methods using SIR-2014,⁴⁶ Fourier analyzed and refined by the full-matrix least-squares based on F^2 implemented in SHELXL-2014.⁴⁷ The Coot program has been used for modelling.⁴⁸ In the final refinement, all non-hydrogen atoms with full occupancy, were treated anisotropically and the hydrogen atoms were included at calculated positions with isotropic $U_{\text{factors}} = 1.2 \cdot U_{\text{eq}}$ or $U_{\text{factors}} = 1.5 \cdot U_{\text{eq}}$ for methyl groups.

Data from a bigger crystal of the dried form of **1** have been corrected for absorption as implemented in the XABS2 program.⁴⁹

5. Conclusions

In conclusion we report on the characterization of a neutral SCO compound capable of switching around room temperature. We proved that compound **1** can be used as a highly-selective material for sensing of methanol and ethanol by a multi-modal response. We showed that corresponding to the spin transition **1** exhibits a simultaneous change of colour, birefringence and Raman spectra, which we exploited in a multi-modal sensor. The transition temperature dramatically changes when **1** is

exposed to methanol or ethanol. Structural details of alcohol adsorption in the crystals and spin transition have been successfully exploited by X-Ray diffraction and interpreted on the atomic scale. We proved that comparing the colour components and the thermal behaviour, we can efficiently distinguish whether a crystallite deposited on a patterned surface was exposed to methanol or ethanol, demonstrating its direct application in TAG sensors.

Despite the facts that the switching of colour and birefringence are particularly intense for compound **1**, they are well-known and common in SCO compounds; this fact allows us to be confident that a similar approach can be extended to many other SCO compounds, enabling new applicative perspective for this class of materials.

Acknowledgements

We thank Massimo Gazzano for fruitful discussion and suggestions and Eva Bystrenova for assembling the figures. The work was partially supported by national flagship project NANOMAX N-CHEM. DG was supported by the EU 7th frame-work program [FP7/2007-2013] under grant agreement no. 280772, project “Implantable Organic Nanoelectronics” (iONE-FP7).

Notes and references

- O. Kahn and C. J. Martinez, *Science*, 1998, **279**, 44–48.
- E. Breuning, M. Ruben, J. M. Lehn, F. Renz, Y. Garcia, V. Ksenofontov, P. Gutlich, E. Wegelius and K. Rissanen, *Angew. Chem., Int. Ed.*, 2000, **39**, 2504.
- P. Gutlich, Y. Garcia and H. A. Goodwin, *Chem. Soc. Rev.*, 2000, **29**, 419–427.
- O. Sato, *Acc. Chem. Res.*, 2003, **36**, 692–700.
- S. Bonhommeau, T. Guillon, L. M. L. Daku, P. Demont, J. S. Costa, J. F. Letard, G. Molnar and A. Bousseksou, *Angew. Chem., Int. Ed.*, 2006, **45**, 1625–1629.
- A. Bousseksou, G. Molnar, P. Demont and J. Menegotto, *J. Mater. Chem.*, 2003, **13**, 2069–2071.
- F. Varret, K. Boukheddaden, E. Codjovi and A. Goujon, *Hyperfine Interact.*, 2005, **165**, 37–47.
- M. Cavallini, *Phys. Chem. Chem. Phys.*, 2012, **14**, 11867–11876.
- M. Cavallini, I. Bergenti, S. Milita, J. C. Kengne, D. Gentili, G. Ruani, I. Salitros, V. Meded and M. Ruben, *Langmuir*, 2011, **27**, 4076–4081.
- E. Coronado, C. Marti-Gastaldo, J. R. Galan-Mascaros and M. Cavallini, *J. Am. Chem. Soc.*, 2010, **132**, 5456–5468.
- P. Gutlich, A. Hauser and H. Spiering, *Angew. Chem., Int. Ed.*, 1994, **33**, 2024–2054.
- A. B. Gaspar and M. Sereyuk, *Coord. Chem. Rev.*, 2014, **268**, 41–58.
- M. A. Halcrow, *Chem. Soc. Rev.*, 2011, **40**, 4119–4142.
- M. A. Halcrow, *Chem. Lett.*, 2014, **43**, 1178–1188.
- M. Nihei, T. Shiga, Y. Maeda and H. Oshio, *Coord. Chem. Rev.*, 2007, **251**, 2606–2621.

- 16 A. Bousseksou, G. Molnar, L. Salmon and W. Nicolazzi, *Chem. Soc. Rev.*, 2011, **40**, 3313–3335.
- 17 M. C. Young, E. Liew and R. J. Hooley, *Chem. Commun.*, 2014, **50**, 5043–5045.
- 18 M. Bartel, A. Absmeier, G. N. L. Jameson, F. Werner, K. Kato, M. Takata, R. Boca, M. Hasegawa, K. Mereiter, A. Caneschi and W. Linert, *Inorg. Chem.*, 2007, **46**, 4220–4229.
- 19 H. L. C. Feltham, C. Johnson, A. B. S. Elliott, K. C. Gordon, M. Albrecht and S. Brooker, *Inorg. Chem.*, 2015, **54**, 2902–2909.
- 20 F. Prins, M. Monrabal-Capilla, E. A. Osorio, E. Coronado and H. S. J. van der Zant, *Adv. Mater.*, 2011, **23**, 1545–1549.
- 21 M. Cavallini, I. Bergenti, S. Milita, G. Ruani, I. Salitros, Z. R. Qu, R. Chandrasekar and M. Ruben, *Angew. Chem., Int. Ed.*, 2008, **47**, 8596–8600.
- 22 V. Meded, A. Bagrets, K. Fink, R. Chandrasekar, M. Ruben, F. Evers, A. Bernand-Mantel, J. S. Seldenthuis, A. Beukman and H. S. J. van der Zant, *Phys. Rev. B: Condens. Matter Mater. Phys.*, 2011, **83**, 245415.
- 23 A. D. Naik, K. Robeyns, C. F. Meunier, A. F. Leonard, A. Rotaru, B. Tinant, Y. Filinchuk, B. L. Su and Y. Garcia, *Inorg. Chem.*, 2014, **53**, 1263–1265.
- 24 J. Linares, E. Codjovi and Y. Garcia, *Sensors*, 2012, **12**, 4479–4492.
- 25 Y. S. Koo and J. R. Galan-Mascaros, *Adv. Mater.*, 2014, **26**, 6785–6789.
- 26 C. Bartual-Murgui, A. Akou, C. Thibault, G. Molnar, C. Vieu, L. Salmon and A. Bousseksou, *J. Mater. Chem. C*, 2015, **3**, 1277–1285.
- 27 B. Schafer, C. Rajnak, I. Salitros, O. Fuhr, D. Klar, C. Schmitz-Antoniak, E. Weschke, H. Wende and M. Ruben, *Chem. Commun.*, 2013, **49**, 10986–10988.
- 28 We identified a minor impurity of a few crystallites (<5%), which contain an excess of ligand in the crystal structure. These crystals do not exhibit spin transition in the range of temperature 170–320 K (above 320 K they decompose).
- 29 G. Brehm, M. Reiher, B. Le Guennic, M. Leibold, S. Schindler, F. W. Heinemann and S. Schneider, *J. Raman Spectrosc.*, 2006, **37**, 108–122.
- 30 D. MasPOCH, D. Ruiz-Molina, K. Wurst, N. Domingo, M. Cavallini, F. Biscarini, J. Tejada, C. Rovira and J. Veciana, *Nat. Mater.*, 2003, **2**, 190–195.
- 31 J. S. Costa, S. Rodríguez-Jiménez, G. A. Craig, B. Barth, C. M. Beavers, S. J. Teat and G. Aromí, *J. Am. Chem. Soc.*, 2014, **136**, 3869–3874.
- 32 C. Genre, G. S. Matouzenko, E. Jeanneau and D. Luneau, *New J. Chem.*, 2006, **30**, 1669–1674.
- 33 A. Kaiba, H. J. Shepherd, D. Fedaoui, P. Rosa, A. E. Goeta, N. Rebbani, J. F. Letard and P. Guionneau, *Dalton Trans.*, 2010, **39**, 2910–2918.
- 34 I. Salitros, O. Fuhr, R. Kruk, J. Pavlik, L. Pogany, B. Schafer, M. Tatarko, R. Boca, W. Linert and M. Ruben, *Eur. J. Inorg. Chem.*, 2013, 1049–1057, DOI: 10.1002/ejic.201201123.
- 35 I. Salitros, J. Pavlik, R. Boca, O. Fuhr, C. Rajadurai and M. Ruben, *CrystEngComm*, 2010, **12**, 2361–2368.
- 36 A. L. Spek, *J. Appl. Crystallogr.*, 2003, **36**, 7–13.
- 37 D. Gentili, M. Durso, C. Bettini, I. Manet, M. Gazzano, R. Capelli, M. Muccini, M. Melucci and M. Cavallini, *Sci. Rep.*, 2013, **3**, 2581.
- 38 M. Cavallini, A. Calo, P. Stoliar, J. C. Kengne, S. Martins, F. C. Maticotta, F. Quist, G. Gbabode, N. Dumont, Y. H. Geerts and F. Biscarini, *Adv. Mater.*, 2009, **21**, 4688–4691.
- 39 D. Gentili, M. Barbalinardo, I. Manet, M. Durso, M. Brucale, A. Mezzi, M. Melucci and M. Cavallini, *Nanoscale*, 2015, **7**, 7184–7188.
- 40 M. Cavallini, D. Gentili, P. Greco, F. Valle and F. Biscarini, *Nat. Protoc.*, 2012, **7**, 1668–1676.
- 41 M. Cavallini, M. Facchini, M. Massi and F. Biscarini, *Synth. Met.*, 2004, **146**, 283–286.
- 42 M. Cavallini, R. Lazzaroni, R. Zamboni, F. Biscarini, D. Timpel, F. Zerbetto, G. J. Clarkson and D. A. Leigh, *J. Phys. Chem. B*, 2001, **105**, 10826–10830.
- 43 P. Leclere, M. Surin, R. Lazzaroni, A. F. M. Kilbinger, O. Henze, P. Jonkheijm, F. Biscarini, M. Cavallini, W. J. Feast, E. W. Meijer and A. Schenning, *J. Mater. Chem.*, 2004, **14**, 1959–1963.
- 44 A. Calo, P. Stoliar, M. Cavallini, Y. H. Geerts and F. Biscarini, *Rev. Sci. Instrum.*, 2010, **81**, 033907.
- 45 W. Kabsch, *Acta Crystallogr., Sect. D: Biol. Crystallogr.*, 2010, **66**, 125–132.
- 46 M. C. Burla, R. Caliendo, M. Camalli, B. Carrozzini, G. L. Cascarano, C. Giacovazzo, M. Mallamo, A. Mazzone, G. Polidori and R. Spagna, *J. Appl. Crystallogr.*, 2012, **45**, 357–361.
- 47 G. M. Sheldrick, *Acta Crystallogr., Sect. A: Found. Adv.*, 2008, **64**, 112–122.
- 48 P. Emsley and K. Cowtan, *Acta Crystallogr., Sect. D: Biol. Crystallogr.*, 2004, **60**, 2126–2132.
- 49 S. Parkin, B. Moezzi and H. Hope, *J. Appl. Crystallogr.*, 1995, **28**, 53–56.